IOPscience iopscience.iop.org

Home Search Collections Journals About Contact us My IOPscience

Detection of sub-ppm traces of aqueous heavy-metal ions using micro-electro-mechanical beam resonators

This content has been downloaded from IOPscience. Please scroll down to see the full text.

2009 J. Micromech. Microeng. 19 115003

(http://iopscience.iop.org/0960-1317/19/11/115003)

View the table of contents for this issue, or go to the journal homepage for more

Download details:

IP Address: 129.110.242.89
This content was downloaded on 03/07/2014 at 16:09

Please note that terms and conditions apply.

J. Micromech. Microeng. **19** (2009) 115003 (7pp) doi:10.1088/0960-1317/19/11/115003

Detection of sub-ppm traces of aqueous heavy-metal ions using micro-electro-mechanical beam resonators

Amir Rahafrooz and Siavash Pourkamali

Department of Electrical and Computer Engineering, University of Denver, Denver, CO 80208, USA

E-mail: spourkam@du.edu

Received 8 March 2009, in final form 27 July 2009
Published 29 September 2009
Online at stacks.iop.org/JMM/19/115003

Abstract
Capacitive silicon micro-mechanical resonators have been utilized in this work as ultra-sensitive mass sensors for the detection of trace amounts of copper ions in water samples. The approach is based on the reduction of aqueous metal ions by the silicon in a resonant structure and consequently deposition of a very thin metal layer on the resonator surface changing its resonant frequency. Measurements demonstrate successful detection of sub-ppm concentrations of copper(II) ions in water. Relatively large frequency shifts (hundreds of ppm) have been measured for resonators exposed to copper concentrations as low as 4 μM (0.26 ppm). An analytical model for the resonant frequency of the resulting complex beams has been derived and used to calculate the thickness of the deposited copper layer based on the measured frequency shifts. The model shows that the measured frequency shifts correspond to only a few atomic layers of copper (as thin as ~7 Å) deposited on the resonator surfaces. This corresponds to a mass sensitivity of more than 4000 Hz μg^{-1} cm^{-2} which is much larger than the highest mass sensitivities measured for quartz crystal microbalances.

(Some figures in this article are in colour only in the electronic version)

1. Introduction

The resonant frequency of micro and nanoscale electromechanical resonators is extremely sensitive to the mass of the resonator. Therefore, such devices can be utilized to measure the mass of a deposited or absorbed material on their surfaces directly with ultimate precision. During the past few years, there have been significant advances and improvements in the performance of silicon-capacitive micro resonators [1, 2]. Such resonators, with their very high quality factors in the tens of thousands, very small sizes and high integration capability can potentially be utilized as ultra-high precision sensors for biomedical diagnosis and chemical detection applications. However, despite extensive speculations very little has been demonstrated using such devices as mass sensors for practical applications.

One of the chemical detection problems that could be attacked with minimal knowledge of chemistry is detection of heavy-metal ions in water samples. Heavy metals such as lead, copper, cadmium, arsenic, etc are critically harmful contaminants of water sources that could occur naturally due to existing minerals in the environment, or as a result of accidents or bioterrorist activities. Such contaminants can produce undesirable health and ecological effects even in extremely small quantities. For example, the World Health Organization specifies a maximum amount of 0.05 mg of lead per liter of drinking water (50 part-per-billion). Traditionally, to detect and avoid such contaminations, water samples are collected and transported to central laboratories for analysis. Most of the current water-monitoring techniques are based on atomic absorption spectroscopy and mass spectrometry [3, 4]. Such techniques require very bulky and power-inefficient equipment for field work and require extremely time-consuming, costly and labor intensive procedures. Therefore, low-cost, portable and easy to use ultra-sensitive sensors for the direct measurement of heavy-metal ions in

 © 2009 IOP Publishing Ltd Printed in the UK

water sources are of great interest [3–5]. Currently, the only available analytical technique suitable for on-site applications is anodic stripping voltammetry which is a very sensitive electrochemical technique [3]. In this technique heavy-metal ions are first deposited on a platinum working electrode at a cathodic potential (preconcentration). The deposited metals are then stripped off by scanning the potential to positive values (stripping). Resulting current generated in the stripping process shows peaks for different metals at different voltages. The position of each peak corresponds to the redox potentials of the respective heavy metal and the height of each peak is proportional to the concentration of the associated heavy-metal ion. Sensitivities in the order of a few ppb (10–100 nM) can be achieved using this technique [3–5]. However, such systems typically require integration of sophisticated mercury electrodes, Ag/AgCl reference electrodes and platinum counting electrodes, making them inconvenient and costly to fabricate and miniaturize using solid-state electronic micro-fabrication technologies [4, 5]. In addition, voltammetry measurements require precise control of pH and conductivity of the solution [5].

The above-mentioned problems in heavy-metal contamination detection, as well as many other unresolved issues in a variety of other chemical and biomedical sensors, can be overcome using micro/nanoscale resonant mass sensor arrays.

As a starting point, here we demonstrate a successful detection of very small concentrations of copper(II) ions in water samples using silicon-capacitive micro resonators. When in contact with the aqueous copper ions, the silicon in the micro-mechanical resonant structure is oxidized by the metallic ions and as a result a very thin metal layer is deposited on the resonator surface changing its mechanical resonant frequency. The existence of targeted metal ions in the sample and their approximate concentration can then be determined by the resulting resonator frequency shift.

2. Resonator fabrication

A single-mask fabrication process was used to fabricate the desired micro resonators in this work. For simplicity and ease of fabrication, we chose one-port clamped-clamped capacitive beam resonators fabricated on silicon-on-insulator (SOI) substrates. Figure 1 shows the fabrication process sequence.

Resonators were fabricated on low-resistivity SOI substrates (device layer resistivity of 0.01 to 0.02 Ω cm) with (100) a few micrometer thick device layers and submicron buffer oxide (BOX) thickness. First, a thin (∼100 nm) layer of silicon dioxide is thermally grown on the silicon substrate. This oxide layer is patterned to the shape of the beam resonators and their wirebonding pads via optical lithography. The resonator structures are then formed by selective anisotropic etching of the device layer of silicon in an aqueous potassium hydroxide (KOH) solution. The resonator structures are defined and protected by the patterned oxide layer on the device layer during this etch step. The beam resonators are aligned to be in parallel or perpendicular to the

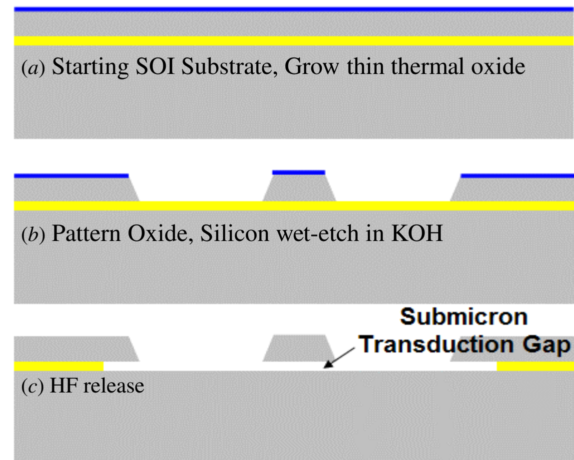

Figure 1. Process flow used for fabrication of the out of plane beam resonators.

1 1 0 direction (main flat of the wafer) of the silicon substrate. Therefore, the resulting sidewalls from anisotropic etching in KOH are 1 1 1 crystalline planes having 54.7° angles with the (1 0 0) silicon surface of the substrate. Although such angled sidewalls affect the resonant frequency of the resonators, they do not interfere with the operation of the beams in their out-of-plane flexural modes and a very clear resonance peak corresponding to the first flexural mode can be detected for the resulting devices. The resonators are then undercut and released in hydrofluoric acid (HF) by etching the underlying silicon dioxide (BOX).

Beam resonators with different dimensions were fabricated on SOI substrates with different device layer thicknesses. Figure 2 shows the SEM view of a fabricated 100 μm long, 20 μm wide (on top) and 9 μm thick beam resonator with a 500 nm capacitive transduction gap.

The capacitive transduction gap lies between the silicon handle layer of the SOI substrate and the beam which is carved in the SOI device layer. Therefore, the size of the gap is determined by the thickness of the buffer oxide layer of the starting SOI substrate and can be much smaller than the lithography limits (potentially as small as a few nanometers).

Due to the orientation alignment requirements, sidewall angles and the need for compensation structures on concave corners, wet anisotropic etching of silicon imposes several challenges and limitations on the shape and consequently the design of the micro and nanoscale devices. However, using this process the structural boundaries and surfaces are defined with atomic level accuracy by the crystalline orientations. This eliminates the surface roughness issues associated with deep reactive ion etching (DRIE) of silicon making wet anisotropic etching of silicon a preferred choice when shrinking the dimensions down to the lower micrometer and nanometer range. Figure 3 is a close-up SEM view of the resonator sidewall showing the extremely smooth surface.

When exposed to the aqueous copper ions, copper atoms with much higher density and lower stiffness replace the silicon atoms on the surface of the resonator reducing its resonant frequency. In the following section, an analytical model is

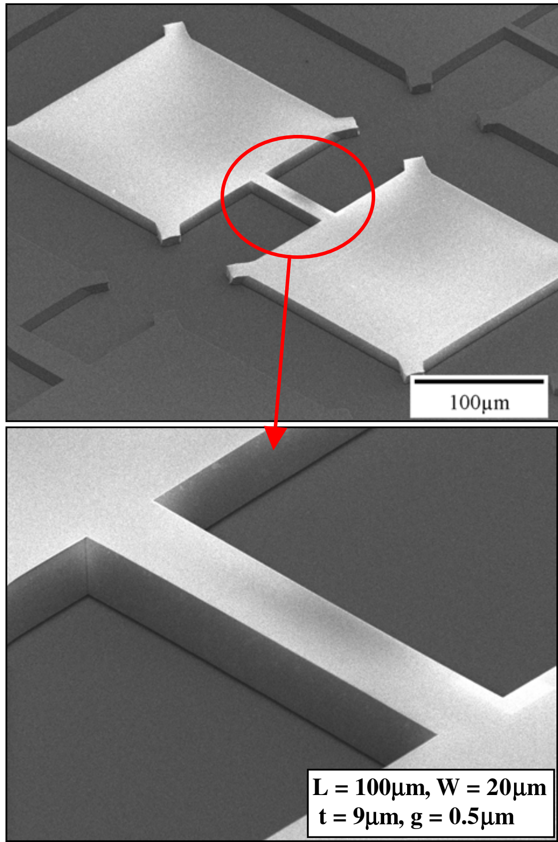

Figure 2. SEM view of a fabricated 100 μm long, 20 μm wide (on-top) and 9 μm thick clamped-clamped beam resonator with a 0.5 μm transduction gap.

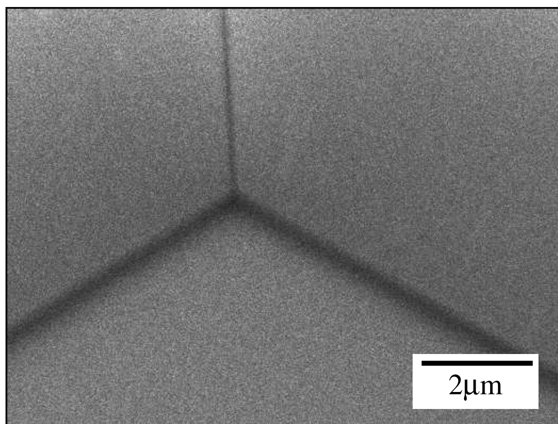

Figure 3. Close-up SEM of the wet-etched resonator sidewall surfaces and the underlying 500 nm transduction gap showing very high smoothness for the sidewalls.

derived for predicting the resulting resonant frequency shift in the fabricated resonators, with trapezoidal cross-section, as a result of copper deposition.

3. Theoretical analysis and modeling

The resonance frequencies of flexural modes of a homogenous clamped-clamped beam resonator can be calculated using equation (1) [6–8]:

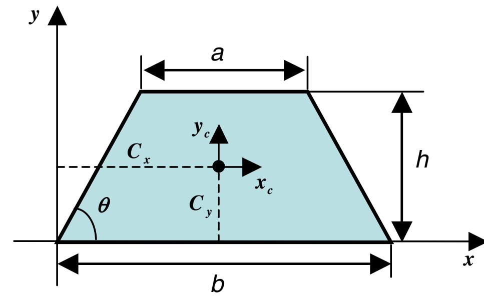

Figure 4. Schematic view of the isoscale trapezoidal cross-section of the fabricated beam resonators.

$$f_n = \frac{\lambda_n^2}{2\pi L^2}\sqrt{\frac{EI}{\rho A}}, \tag{1}$$

where n is the resonance mode number, ρ, A, L, E and I are the density, cross-sectional area, length, Young's modulus and the moment of inertia of the beam, respectively. λ_n is the frequency coefficient for each resonance mode and can be calculated by solving equation (2):

$$\cos(\lambda_n)\cosh(\lambda_n) = 1. \tag{2}$$

Numerically solving equation (2) results in the following λ_n values for the first three flexural resonance modes of the beam: $\lambda_1 = 4.731$, $\lambda_2 = 7.854$ and $\lambda_3 = 10.996$.

Considering that the beam resonators in this work have isoscale trapezoidal cross-sections (figure 4), the area moment of inertia about the x_c axis (the horizontal line passing through the center of mass) can be calculated as follows:

$$I_{x_c} = \frac{h^3(a^2 + 4ab + b^2)}{36(a + b)}, \tag{3}$$

where h is the beam thickness, a and b are the upper and lower widths of the beam and θ is the angle between the lateral walls and the horizontal line, having a value of $\theta = 54.7^\circ$ in this case. Having θ and a (lithographically defined resonator upper width), the value of b can be calculated as follows:

$$b = a + 2h\cot(\theta), \tag{4}$$

and the location of the center of mass of a trapezoid is

$$(C_x, C_y) = \left(\frac{b}{2}, \frac{h(2a + b)}{3(a + b)}\right). \tag{5}$$

Replacing equation (3) for the moment of inertia in (1) and using $\lambda_1 = 4.731$, one can calculate the first flexural resonance mode of a clamp-clamp beam resonator with isoscale trapezoid cross-section.

After deposition of copper on the beam surfaces, in order to calculate the resonance frequency of the resulting composite beam, the bending stiffness EI and density ρ in equation (1) can be replaced, with a good approximation, by the composite bending stiffness $\bar{E}\bar{I}$ and density $\bar{\rho}$ [9] given by the following equations:

$$\bar{E}\bar{I} = E_{Si}I_{Si} + E_{Cu}I_{Cu}, \tag{6}$$

$$\bar{\rho} = \frac{\rho_{Si}A_{Si} + \rho_{Cu}A_{Cu}}{A_{Si} + A_{Cu}}. \tag{7}$$

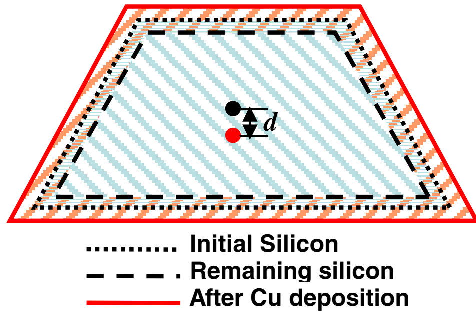

Figure 5. The schematic view of the isoscale trapezoidal cross-section of a composite beam resulting from the reaction of the aqueous copper ions with silicon. A thin layer of silicon on the surface is dissolved and replaced by copper (the red dashed part). The black and red circles show the center of mass for the silicon (shown in blue) and copper (shown in red) parts, respectively.

To find I_{Si} and I_{Cu} with respect to the horizontal line that passes through the overall center of mass, the moments of inertia around the center of mass of each part is calculated first. Equation (8) can then be used to find the moments of inertia around the overall center of mass of the beam:

$$I_i = I_{x_c} + Ad_i^2, \tag{8}$$

where I_i represent the moment of inertia about a new horizontal line called i. d_i is the distance between horizontal lines $x_c$and i and A is the cross-sectional area.

Figure 5 shows the cross-sectional view of the beam resonator after replacement of its outer silicon layer with a copper layer. The next steps include finding the moment of inertia for each of these parts about the horizontal lines that pass through their slightly different centers of mass (black and red circles in figure 5) and then finding the overall center of mass. Equation (8) will then be utilized to recalculate moments of inertia around the horizontal line passing through the overall center of mass.

As a result of the reaction between copper (II) ions and silicon, a thin layer of silicon t_{Si} will be removed and dissolved in the solution while a thin layer of copper t_{Cu} will replace it. The resulting new dimensions of the trapezoidal cross-sections of silicon and copper parts of the beam can be calculated as follows:

$$a_{\mathrm{Si}} = a - 2t_{\mathrm{Si}} \tan\left(\frac{\theta}{2}\right) \tag{9}$$

$$b_{\mathrm{Si}} = b - 2t_{\mathrm{Si}} \cot\left(\frac{\theta}{2}\right) \tag{10}$$

$$h_{\mathrm{Si}} = h - 2t_{\mathrm{Si}}, \tag{11}$$

and

$$a_{\mathrm{Cu}} = a + 2(t_{\mathrm{Cu}} - t_{\mathrm{Si}}) \tan\left(\frac{\theta}{2}\right), \tag{12}$$

$$b_{\mathrm{Cu}} = b + 2(t_{\mathrm{Cu}} - t_{\mathrm{Si}}) \cot\left(\frac{\theta}{2}\right), \tag{13}$$

$$h_{\mathrm{Cu}} = h + 2(t_{\mathrm{Cu}} - t_{\mathrm{Si}}). \tag{14}$$

Table 1. Material properties for silicon and copper.

Material	m_a (g mol^{-1})	ρ (kg m^{-3})	E (GPa)
Si	28.0855	2330	150
Cu	63.546	8960	128

I_{Si} and I_{Cu} can now be calculated about the horizontal lines passing through their centers of mass as below:

$$I_{\mathrm{Si}} = \frac{h_{\mathrm{Si}}^3\left(a_{\mathrm{Si}}^2 + 4a_{\mathrm{Si}}b_{\mathrm{Si}} + b_{\mathrm{Si}}^2\right)}{36(a_{\mathrm{Si}} + b_{\mathrm{Si}})}, \tag{15}$$

$$I_{\mathrm{Cu}} = \frac{h_{\mathrm{Cu}}^3\left(a_{\mathrm{Cu}}^2 + 4a_{\mathrm{Cu}}b_{\mathrm{Cu}} + b_{\mathrm{Cu}}^2\right)}{36(a_{\mathrm{Cu}} + b_{\mathrm{Cu}})} - \left[\frac{h_{\mathrm{Si}}^3\left(a_{\mathrm{Si}}^2 + 4a_{\mathrm{Si}}b_{\mathrm{Si}} + b_{\mathrm{Si}}^2\right)}{36(a_{\mathrm{Si}} + b_{\mathrm{Si}})} + A_{\mathrm{Si}}d^2\right], \tag{16}$$

where $A_{\mathrm{Si}} = \frac{h_{\mathrm{Si}}}{2}(a_{\mathrm{Si}} + b_{\mathrm{Si}})$ is the trapezoidal area of the silicon part and d is the distance between copper and silicon centers of mass and equals

$$d = C_{y_{\mathrm{Si}}} - C_{y_{\mathrm{Cu}}} = \left(\frac{h_{\mathrm{Si}}(2a_{\mathrm{Si}} + b_{\mathrm{Si}})}{3(a_{\mathrm{Si}} + b_{\mathrm{Si}})} + t_{\mathrm{Cu}}\right) - \frac{h_{\mathrm{Cu}}(2a_{\mathrm{Cu}} + b_{\mathrm{Cu}})}{3(a_{\mathrm{Cu}} + b_{\mathrm{Cu}})}. \tag{17}$$

The overall center of mass is

$$C_T = \frac{\rho_{\mathrm{Si}}A_{\mathrm{Si}}C_{y_{\mathrm{Si}}} + \rho_{\mathrm{Cu}}A_{\mathrm{Cu}}C_{y_{\mathrm{Cu}}}}{\rho_{\mathrm{Si}}A_{\mathrm{Si}} + \rho_{\mathrm{Cu}}A_{\mathrm{Cu}}}. \tag{18}$$

The moments of inertia around the line passing through the overall center of mass using equations (8), (15), (16), (17) and (18) are

$$I_{\mathrm{Si}_T} = I_{\mathrm{Si}} + A_{\mathrm{Si}}\left(C_{y_{\mathrm{Si}}} - C_T\right)^2, \tag{19}$$

$$I_{\mathrm{Cu}_T} = I_{\mathrm{Cu}} + A_{\mathrm{Cu}}\left(C_T - C_{y_{\mathrm{Cu}}}\right)^2. \tag{20}$$

The ratio of the thickness of deposited Cu and removed Si can be calculated based on their atomic masses and densities. For every silicon atom that is removed, two copper atoms are deposited. Therefore, the volume ratio between Cu and Si is

$$\frac{V_{\mathrm{Cu}}}{V_{\mathrm{Si}}} = \frac{2m_{a_{\mathrm{Cu}}}/\rho_{\mathrm{Cu}}}{m_{a_{\mathrm{Si}}}/\rho_{\mathrm{Si}}}, \tag{21}$$

where V_{Cu}, V_{Si}, $m_{a_{\mathrm{Cu}}}$ and $m_{a_{\mathrm{Si}}}$ are the volumes of deposited copper and removed silicon, and atomic masses of copper and silicon, respectively. Table 1 contains the atomic mass and density values for silicon and copper. Since the surface area is almost the same for both copper and silicon, this ratio is also equal to the ratio of their thicknesses:

$$\frac{t_{\mathrm{Cu}}}{t_{\mathrm{Si}}} = \frac{V_{\mathrm{Cu}}}{V_{\mathrm{Si}}} = \frac{2m_{a_{\mathrm{Cu}}}/\rho_{\mathrm{Cu}}}{m_{a_{\mathrm{Si}}}/\rho_{\mathrm{Si}}} = 1.1767. \tag{22}$$

Using the equations derived in this section and based on the measured changes in the resonance frequency of the clamp-clamp beam resonators after copper deposition, one can find the thickness of the deposited copper. According to equations (6) and (7), the resonance frequency of the beam has a nonlinear dependence on the thickness of the deposited

Table 2. Summary of measurement results obtained from several resonators with different dip times in water samples with various copper concentrations.

Resonator Dimensions L/W/H (μm)	Freq. (MHz)	Q. Factor (in air)	Copper concent. (μM)	Copper conc. (ppm)	Dip time (min)	Freq. shift (kHz)	Freq. shift (ppm)	t_{Cu} (nm)	~# Cu Atomic layers deposited
100/20/9	4.9718	200	1000	64	5	−17.4	−3500	7.48	24
100/10/9	5.2041	140	1000	64	5	−20.2	−3880	7.03	32
100/5/9	5.3900	80	1000	64	5	−34.8	−6460	9.98	53
150/10/9	2.6964	50	1000	64	5	−11.4	−4230	7.66	35
100/10/9	5.3538	190	400	26	10	−29	−5420	9.84	45
150/20/9	2.7353	120	400	26	10	−10	−3660	7.81	30
150/10/9	2.7212	55	400	26	10	−12.5	−4590	8.33	37
100/10/9	5.4022	110	40	2.6	5	−2.5	−460	0.83	4
150/20/9	2.7148	110	40	2.6	5	−1.5	−550	1.17	5
100/10/5	3.6591	90	10	0.64	10	−2.6	−710	0.82	3
100/5/5	3.5689	50	10	0.64	10	−4.3	−1200	1.18	5
100/20/9	5.0460	140	4	0.26	10	−2.4	−440	1.01	4
100/10/9	5.1812	150	4	0.26	10	−2.0	−390	0.70	3

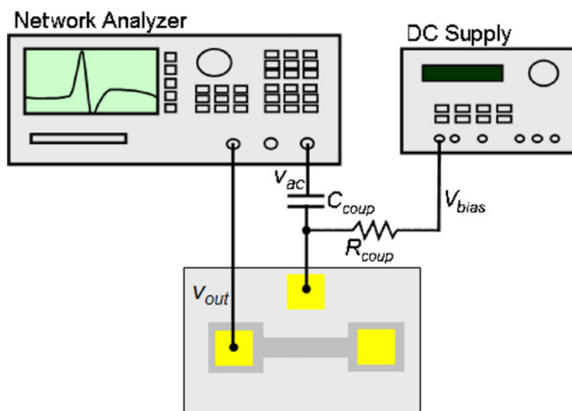

Figure 6. Schematic diagram of the test setup and electrical connections to the beam resonators for one-port operation and frequency response measurement.

copper layer. Since the derivation of an analytical closed-form solution for the calculation of the deposited copper thickness based on the measured frequency shift is not a trivial task and out of the main focus of this work, a numerical method has been adopted for this purpose. Therefore, a MATLAB code was developed to calculate the change in frequency for different deposited copper thicknesses based on the resonator dimensions. The assumed copper thickness starts from a very small value (~0) and keeps increasing with very small increments until the resulting change in frequency is equal to or greater than the measured value. Since the smallest deposited copper thicknesses in our experiments are in the order of a few angstroms, a step size of 10 pm was chosen. The calculated copper thicknesses using this method are reported in table 2.

4. Experiments and measurement results

The fabricated beam resonators can be operated in a one-port configuration, where the SOI handle layer acts as the actuation electrode. Figure 6 shows the schematic diagram of the test setup used to measure the frequency response of the resonators. Electrical connections to the resonators were made by connecting aluminum wires between the silicon pads and the metal tracks on a printed circuit board (using a wedge bonder). A dc bias voltage (V_{bias}) in addition to the ac actuation signal from the network analyzer are applied to the handle layer while the output current is collected from the resonator body (figure 6). To decouple the dc and ac signal paths to the sources, the dc bias was applied through a large resistor (100 kΩ) and the ac signal was applied through a relatively large capacitor (1 μF).

The ac signal on top of the DC bias generates a fluctuating electrostatic force applied to the beam by the handle layer that causes vertical (out of plane) mechanical vibrations in the beam. The current induced in the beam (output signal) is a function of the dc bias voltage and the vibration amplitude of the resonator. The vibration amplitude is amplified by a factor of Q (quality factor of the resonator at the mechanical resonant frequency of the beam, 2–6 MHz in this work depending on the beam dimensions) resulting in a sharp increase in the output signal. The frequency response of the resonators can be measured by connecting the resonator body to the input of a network analyzer that measures and graphs the resulting output current as a function of frequency.

After precise measurement of the resonance frequencies of the fabricated devices, the samples were dipped in copper(II)-sulfate solutions with different concentrations ranging from 1 mM to 4 μM. Figure 7 demonstrates the electrochemical reactions between the crystalline silicon in the resonator structure and the copper(II) ions in the solution. Silicon has a relatively low redox potential and therefore it can be oxidized by almost all the heavy-metal ions of interest. The reaction includes oxidation of silicon into silicon dioxide and reduction of the metal ions to neutral metallic atoms, and subsequently deposition of a metal layer on the silicon surface. To facilitate and accelerate the reaction, a few drops of buffered HF were added to the solutions. Fluoride ions in the solution absorb the oxidized silicon atoms into the solution (in the form of a water soluble complex ion SiF_6^{-2}) and avoid the formation of insulating silicon dioxide thin films on the silicon surfaces (figure 7).

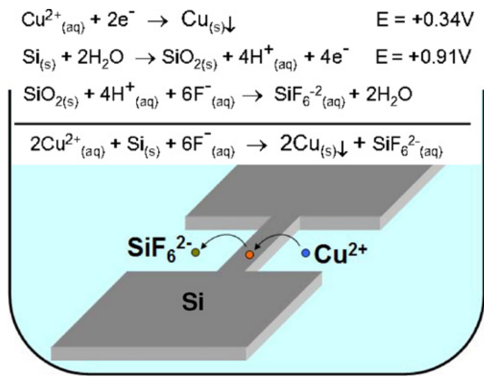

Figure 7. Schematic diagram of the electrochemical reaction between the silicon atoms on the surface of the resonator and copper (II) ions resulting in the deposition of copper on the resonator surfaces.

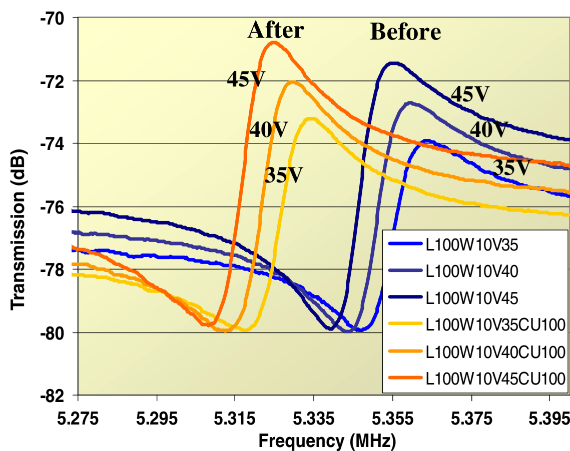

Figure 8. Measured frequency response of a 5.3 MHz c-c beam resonator with different bias voltages before and after dipping in a water sample containing 26 ppm of copper (II) ions for 10 min showing ∼29 kHz of frequency reduction.

After a few minutes (5–10) in the solution, the resonators were rinsed and dried and their resonant frequencies were measured again. Figures 8 and 9 show measured frequency responses for two resonators before and after exposure to the copper solutions with different concentrations. The graphs clearly show a decrease in the resonant frequency of the resonators after dipping in the copper (II) solutions.

Table 2 summarizes several measurement results obtained from different resonators in solutions with different copper concentrations and dip times. To ensure that the observed resonator frequency shifts are a result of interactions with the copper (II) ions in the solution, we repeated similar tests in DI water, diluted hydrofluoric acid (HF) and diluted buffered HF solutions. No measurable shift in the resonant frequency of the resonators was observed after washing and drying the samples. Furthermore, the trends in the measurement results clearly show a correlation between the resonator frequency shifts and the copper concentrations and dip times confirming that the observed frequency shifts are resulting from the copper ions in the solutions.

The other parameter that needs to be taken into account in this work is the temperature-induced frequency drift of the resonators. As shown in [10], single crystalline silicon resonators have a temperature coefficient of frequency (TCF) of -27.8 ppm $^\circ C^{-1}$. Considering the fact that even the smallest measured frequency drifts, in table 2, are in the hundreds of ppm range, and all the experiments were performed in an air-conditioned environment with a temperature control precision of at least ± 1 °C, the measured frequency shifts cannot be due to temperature. However, for higher precision measurements and achieving the phase noise limited frequency measurement accuracy limits for high-Q resonators, a high precision temperature control for the resonators will be required.

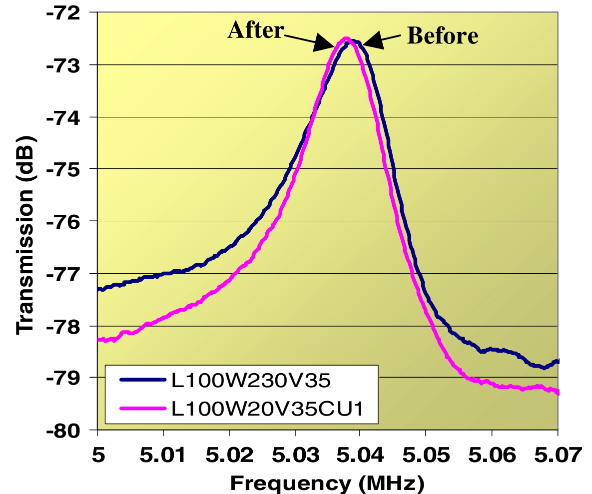

Figure 9. Measured frequency response of a 5 MHz resonator showing ∼2.4 kHz of shift after a 10 min dip in a 0.26 ppm copper solution.

The last column in table 2 includes the calculated copper thickness based on the measured frequency shifts and by numerically solving the set of equations derived in section III. Sub-nanometer copper thicknesses equivalent to only ∼3–4 atomic layers of copper have been successfully measured by the resonators. The measured frequency shifts even for sub-ppm concentrations of copper are orders of magnitude higher than the frequency measurement accuracy limits for such resonators when incorporated in a low-noise oscillator configuration [11]. Therefore, resolutions in the ppb range are expected to be easily achievable using such resonators.

The measured data shows mass sensitivities as high as 4000 Hz μg^{-1} cm^{-2} for the clamped-clamped resonators in this work which is higher than the typical range of 10–2000 Hz μg^{-1} cm^{-2} for quartz crystal microbalances [11]. Orders of magnitude higher mass sensitivities can be achieved for higher frequency bulk mode silicon micro resonators [1].

5. Conclusions and future work

Capacitive silicon resonators were utilized as ultra-sensitive mass sensors for the detection of trace amounts of copper(II) ions in water samples. Preliminary measurements in this work demonstrate successful detection of sub-ppm concentrations

of copper(II) ions in water. Frequency shifts as high as ∼400 ppm have been measured for resonators exposed to copper concentrations as low as 4 μM (0.26 ppm). This corresponds to only a few atomic layers of copper (∼5 Å thick) deposited on the resonator surface.

Furthermore, an array of resonators coated with different metals or connected to different electrical potentials can be utilized for simultaneous selective detection of more than one metal in water samples.

Future work includes the incorporation of micro-resonant mass sensors in a low-noise oscillator configuration to achieve frequency resolutions in a few Hz range enhancing the sensor resolution to concentrations as low as a few ppb. Furthermore, arrays of resonators coated with different metals or connected to different electrical potentials will be used for simultaneous detection of more than one metal in a sample.

References

[1] Pourkamali S *et al* 2007 Low-impedance VHF and UHF capacitive silicon bulk acoustic wave resonators, part I: concept and fabrication *IEEE Trans. Electron. Devices* **54** 2017–23

[2] Pourkamali S *et al* 2003 High-Q single crystal silicon HARPSS capacitive beam resonators with self-aligned sub-100 nm transduction gaps *J. Micro Electro Mech. Syst.* **12** 487–96

[3] Zou S *et al* 2007 An environmental automatic monitoring system for heavy metals *Proc. IEEE Int. Conf. on Control and Automation (30 May–1 June 2007)* 798–801

[4] Yun K-S *et al* 2003 A miniaturized low-power wireless remote environmental monitoring system using microfabricated electrochemical sensing electrodes *Proc. 12th IEEE Int. Conf. on Solid-State Sensors, Actuators and Microsystems (TRANSDUCERS) (8–12 June 2003)* pp 1867–70

[5] Zhu X-S *et al* 2003 Mercury droplet microelectrode sensor on lab-on-a-chip for heavy metal ion detection *Proc. 12th IEEE Int. Conf. on Solid-State Sensors, Actuators and Microsystems (TRANSDUCERS) (8–12 June 2003)* pp 61–4

[6] Shabana A A 1991 *Theory of Vibration* (Berlin: Springer)

[7] Genta G 1998 *Vibration of Structures and Machines* 3rd edn (Berlin: Springer)

[8] Weaver W Jr, Timoshenko S P and Young D H 1989 *Vibration Problems in Engineering* 5th edn (New York: Wiley)

[9] Voiculescu I R *et al* 2006 Modelling and measurements of a composite microcantilever beam for chemical sensing applications *J. Mech. Eng. Sci.*

[10] Pourkamali S, Ho G K and Ayazi F 2007 Low-impedance VHF and UHF capacitive silicon bulk acoustic wave resonators, part II: measurement and characterization *IEEE Trans. Electron. Devices* **54** 2024–30

[11] Rodriguez-Pardo L *et al* 2005 Sensitivity, noise, and resolution in QCM sensors in liquid media *IEEE Sensors J.* **5** 1251–7